Incommensurate spin-density-wave and metal-insulator transition in the one-dimensional periodic Anderson model

P. R. Bertussi,[1] M. B. Silva Neto,[1] T. G. Rappoport,[1] A. L. Malvezzi,[2] and R. R. dos Santos[1]

[1]*Instituto de Física, Universidade Federal do Rio de Janeiro, Caixa Postal 68528, 21941-972 Rio de Janeiro RJ, Brazil*

[2]*Departamento de Física, Faculdade de Ciências, Universidade Estadual Paulista, Caixa Postal 473, 17015-970 Bauru SP, Brazil*

(Received 16 February 2011; revised manuscript received 15 April 2011; published 15 August 2011)

We have used the density-matrix renormalization group method to study the ground-state properties of the symmetric periodic Anderson model in one dimension. We have considered lattices with up to $N_s = 50$ sites, and electron densities ranging from quarter to half filling. Through the calculation of energies, correlation functions, and their structure factors, together with careful extrapolations (toward $N_s \to \infty$), we were able to map out a phase diagram U vs n, where U is the electronic repulsion on f orbitals, and n is the electronic density, for a fixed value of the hybridization. At quarter filling, $n = 1$, our data is consistent with a transition at $U_{c_1} \simeq 2$, between a paramagnetic (PM) metal and a spin-density-wave (SDW) insulator; overall, the region $U \lesssim 2$ corresponds to a PM metal for all $n < 2$. For $1 < n \lesssim 1.5$ a ferromagnetic phase is present within a range of U, while for $1.5 \lesssim n < 2$, we find an incommensurate SDW phase; above a certain $U_c(n)$, the system displays a Ruderman-Kittel-Kasuya-Yosida behavior, in which the magnetic wave vector is determined by the occupation of the conduction band. At half filling, the system is an insulating spin liquid, but with a crossover between weak and strong magnetic correlations.

DOI: 10.1103/PhysRevB.84.075156 PACS number(s): 71.10.Fd, 71.27.+a, 71.30.+h

I. INTRODUCTION

The periodic Anderson model (PAM)[1] is believed to be the minimal model describing the essential physics of heavy-fermion systems.[2] In these systems, the proximity of an incomplete f level, due to rare-earth or actinide atoms, to a d band from transition-metal ions, leads to an increased effective mass for the conduction electrons, which can reach up to a thousand times its bare mass. The model is thus composed of two bands: a conduction band, in which the electrons can hop between neighboring sites with hopping energy t, and local f states at each site, which are taken as dispersionless and nondegenerate (i.e., these local states only accommodate up to two electrons of opposite spin orientations); two electrons occupying the same f state feel a Coulomb repulsion U. Finally, a hybridization term, of magnitude V, couples these two bands, and one often considers the particle-hole-symmetric case, in which the energy of the localized orbital is $\varepsilon_f = -U/2$. The Hamiltonian is defined in Eq. (1) below.

The overall physics of the one-dimensional model, which is our concern here, has been known for some time. Starting from the strong-coupling regime, $U \gg 4t$, and without hybridization, the ground state at quarter filling, $n = N_e/N_s = 1$ (where N_e and N_s are the number of electrons and number of sites, respectively), corresponds to single occupation of the f orbitals, which is highly degenerate in spin. When the hybridization V is switched on, an effective exchange interaction between neighboring f electrons lifts this degeneracy: each electron leaks to the conduction band, hops to a neighboring site, and ends up on the f orbital adjacent to where it started such virtual process; it is therefore a sixth-order process, amounting to an exchange energy $J_1 \sim t^2V^4/|\varepsilon_f|^5$, which favors an antiferromagnetic alignment between neighboring spins.[3,4] Further, in this strong-coupling regime, the system is a charge-transfer insulator, and as U decreases, an insulator-to-metal transition takes place at some U_{c1}, as discussed in Ref. 5; however, as far as we know, no reliable estimates for U_{c1} have been given to date. At half filling, on the other hand, the ground state has been proven to be a singlet,[6] with short-ranged antiferromagnetic correlations;[7] strong coupling corresponds to the Kondo regime, in which charge fluctuations are negligible, whereas weak coupling represents the intermediate-valence regime, in which charge fluctuations are important, and the leaking of electrons from the f orbitals tends to suppress antiferromagnetic correlations.[8,9] For quarter filling plus one electron, it has been shown that, if the f level is deep enough, the state is ferromagnetic.[5] Most of the knowledge in the regime of intermediate fillings, $1 < n < 2$, comes from numerical work, although the large number of states per lattice site (16) has hindered unbiased analyses of the model over the years, even in one spatial dimension.

The development of the density-matrix renormalization group (DMRG) method[10–14] allowed numerical results for the PAM on moderately large systems to be obtained for arbitrary densities. Some magnetic properties of the model have been unveiled,[8,15,16] from which a ground-state phase diagram $U \times n$ (for fixed hybridization V, and for $1 \leqslant n \leqslant 2$) has been proposed, with the following features: (1) For small U the system is paramagnetic for all n between quarter and half filling. (2) For $n = 1$ the system has strong antiferromagnetic correlations for large values of U. (3) Near quarter filling, ferromagnetic (FM) phases emerge, in which the total spin S has been predicted[15] to be $0 < S/N_s < (1 - n_c)/2$, where n_c is the conduction electron density; for definiteness, note that it is not the latter which is controlled independently, but the *total* density, $n = n_c + n_f$. (4) As the filling is increased, these FM phases give way to a phase with $S = 0$, but with Ruderman-Kittel-Kasuya-Yosida (RKKY)[17–19] correlations, i.e., characterized by the magnetic structure factor being peaked at $2k_F^c$, where k_F^c is the Fermi wave vector of the conduction band in the noninteracting case, i.e., with $V = 0$.[15]

However, in spite of the many advances, some important issues related to the phase diagram remain unanswered, or in need of more thorough analyses. As mentioned above, an estimate of U_{c1}, the metal-insulator critical point at quarter filling, must be obtained. Also, the boundaries of the ferromagnetic phase must be more accurately determined. Furthermore, a slave-boson mean-field analysis[4] of the model predicted a spiral incommensurate phase, which was not confirmed by early DMRG calculations;[15] given that these calculations were restricted to $N_s \leqslant 24$ sites, this issue must also be carefully scrutinized. By the same token, the nature of the different regimes at half filling must be further clarified.

With the purpose of advancing knowledge into these issues, here we study the PAM through the DMRG approach, considering lattices up to 50 sites. With larger systems, we have been able to obtain the spatial decay of magnetic correlations, as well as high-resolution magnetic structure factor data (i.e., up to 50 k points in the Brillouin zone); as a result, in addition to determining the phase boundaries more accurately than before, an intermediate incommensurate spin-density wave is found to occupy a significant portion of the phase diagram. We have also been able to generate data for the charge gap, from which reliable extrapolations to $N_s \to \infty$ could be performed, thus distinguishing metallic and insulating regions of the phase diagram. The paper is organized as follows. In Sec. II we present the model and lay out some calculational details. In Secs. III, IV, and V we present our results for half filling, quarter filling, and for intermediate fillings, respectively. The phase diagram is presented in Sec. VI, together with our final conclusions.

II. MODEL AND CALCULATIONAL PROCEDURE

The periodic Anderson model is defined by the Hamiltonian

$$H = -t \sum_{i\sigma} (c^\dagger_{i\sigma} c_{i+1\sigma} + c^\dagger_{i+1\sigma} c_{i\sigma}) + \varepsilon_f \sum_{i\sigma} n^f_{i\sigma} + U \sum_i n^f_{i\uparrow} n^f_{i\downarrow} + V \sum_{i\sigma} (c^\dagger_{i\sigma} f_{i\sigma} + f^\dagger_{i\sigma} c_{i\sigma}), \quad (1)$$

where $c^\dagger_{i\sigma}$ ($f^\dagger_{i\sigma}$) and $c_{i\sigma}$ ($f_{i\sigma}$) are the creation and annihilation operators for electrons in the conduction (localized) band; $n_{i\sigma} = f^\dagger_{i\sigma} f_{i\sigma}$ is the number operator of the localized f electrons. t is the nearest-neighbor hopping integral, U is the (on site) Coulomb repulsion for two localized electrons on the same site, V is the hybridization between the conduction and f bands, and ε_f is the energy displacement of the localized band. Since we are dealing with the symmetric case, we set $\varepsilon_f = -U/2$.

We have used the finite DMRG method with open boundary conditions to obtain the ground state $|\Psi_0\rangle$ and energy $E_0(N_e)$, where N_e is the number of electrons for electronic densities from $n \equiv N_e/N_s = 1$ to 2, where N_s is the number of sites. We have generated chains with up to 50 sites with a discarded weight of 10^{-5} to 10^{-9} in the final sweep. The hopping parameter t was set to 1 and defines the energy scale. The hybridization constant is fixed at 0.75, in order to compare with previous results (which used $t = 0.5$ and $V = 0.375$),[15] while the Coulomb parameter ranges from $U = 0$ to $U = 20$.

A. Charge gap and metal-insulator transitions

In order to search for metal-insulator transitions we make use of the charge gap,[20]

$$\Delta_c = E_0(N_e + 1) + E_0(N_e - 1) - 2E_0(N_e), \quad (2)$$

which is also referred to as the quasiparticle gap.[8] For each set of parameters in the Hamiltonian, we have calculated this gap for at least three different system sizes N_s plotted against $1/N_s$, and using a linear fit, obtained the extrapolated value for Δ_c when $N_s \to \infty$. In the figures below, the error bars of the extrapolated charge gaps are smaller than the data points.

B. Spin-correlation functions and structure factors

The characterization of the magnetic arrangements in each band is achieved by calculating the real-space correlation functions,

$$S^\alpha(r) = \langle \mathbf{S}^\alpha_i \cdot \mathbf{S}^\alpha_{i+r} \rangle, \quad (3)$$

and their structure factors,

$$\tilde{S}^\alpha(k) = \frac{1}{N_s} \sum_{i,j} e^{ik(i-j)} \langle \mathbf{S}^\alpha_i \cdot \mathbf{S}^\alpha_j \rangle, \quad (4)$$

where the index $\alpha = c, f$ runs over the two bands, $\mathbf{S}^c_i \equiv \sum_{\alpha,\beta=\pm} c^\dagger_{i\alpha} \boldsymbol{\sigma}_{\alpha\beta} c_{i\beta}$ ($\boldsymbol{\sigma}$ are the Pauli matrices), $\mathbf{S}^f_i \equiv \sum_{\alpha,\beta=\pm} f^\dagger_{i\alpha} \boldsymbol{\sigma}_{\alpha\beta} f_{i\beta}$, $\langle \ldots \rangle \equiv \langle \Psi_0 | \cdots | \Psi_0 \rangle$, and in order to minimize edge effects due to our open boundary conditions, we discard site-dependent data within five sites at each end. We have also examined how the peak heights of the structure factors change with lattice size. Their increase with N_s indicates that the correlations are "long ranged," as opposed to having a constant value if correlations are short ranged.[21] However, one should have in mind that, since the model has SU(2) symmetry and our results are restricted to one dimension, no true long-range *order* is possible.

C. Hybridization and on-site correlations

Other quantities of interest are the hybridization correlation,

$$T_{cf} = \frac{1}{N_s} \sum_{i,\sigma} \langle c^\dagger_{i\sigma} f_{i\sigma} + f^\dagger_{i\sigma} c_{i\sigma} \rangle, \quad (5)$$

and the on-site correlation between c- and f-band electronic spins,

$$S_{cf} = \frac{1}{N_s} \sum_i \langle \mathbf{S}^c_i \cdot \mathbf{S}^f_i \rangle, \quad (6)$$

which is a measure of the magnetic coupling between the bands. Since both the hybridization and the on-site magnetic correlations are always negative in our data, in what follows we show their absolute values.

III. HALF FILLING ($n = 2$)

We start by recalling the behavior for the free case, i.e., $U = 0$. In this case, the Hamiltonian is quadratic in the c and

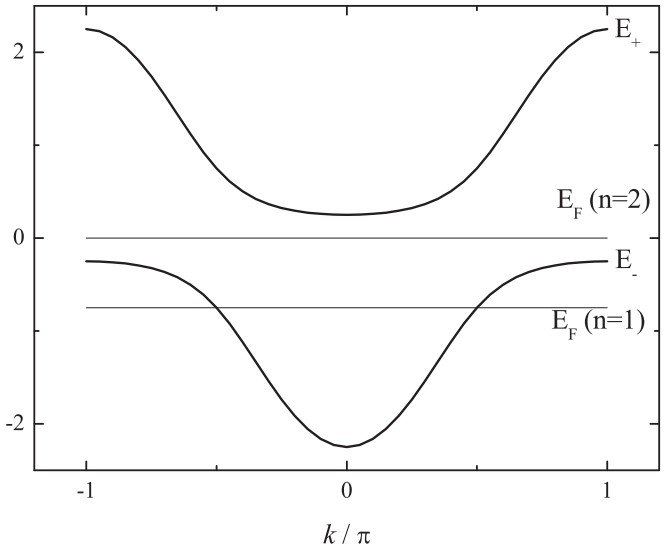

FIG. 1. The dispersion relations, Eq. (7), for the free case, and for $V = 0.75$.

f fields, and can be easily diagonalized in k space to yield the eigenvalues

$$E_{\pm}(k) = \frac{\varepsilon_c(k) \pm \sqrt{[\varepsilon_c(k)]^2 + 4V^2}}{2}, \tag{7}$$

where $\varepsilon_c(k) = -2t \cos k$, with the lattice spacing being set to unity. These eigenvalues are plotted in Fig. 1. At half filling, only the lower band is occupied, so the Fermi energy lies within the hybridization gap: the system is therefore a paramagnetic insulator when $U = 0$.

When the on-site repulsion on the f orbitals is switched on, the charge gap remains finite for all values of U, as shown by our DMRG data in Fig. 2(a). However, the nonmonotonic behavior observed in the charge gap reveals that the large-U regime is somewhat different from the small-U regime: the gap increases with U up to $U^{\times} \simeq 2.2$, where it reaches a maximum, and then decreases steadily above $U^{\times}$, in qualitative agreement with early calculations for different sets of parameters.[8,22]

The origin of this nonmonotonic behavior can be understood through a simple mean-field, Hartree-Fock (HF), analysis, which shows that the system goes from a paramagnetic solution to an antiferromagnetic solution with the increase of U. Data for the charge gap thus obtained is plotted in Fig. 2(a) for comparison with our DMRG results. For small values of U, the gap involves states with predominantly f character, and as U increases, the energy difference between the states above and below the Fermi level is enlarged, leading to an increase of the gap. Beyond the maximum of the gap, the character of this state changes from f to mostly c band; in this regime, states with predominant f character lie well below the Fermi level and there is a reduction of the gap led by the decrease of the effective hybridization with U (see below). Given that our DMRG data are in good agreement with this HF analysis, a more thorough examination of the magnetic correlations with U is in order; the discrepancy of the data near $U^{\times}$ should be attributed to quantum fluctuations not captured by the HF approximation.

First, we note that the signature of the crossover is also present in the behavior of the hybridization and on-site magnetic correlations, Eqs. (5) and (6), shown in Fig. 2(b). In the half-filled case, the occupation of each band is independent of U and is equal to one electron per site. Also, as U increases (and also the magnitude of ε_f), the cost of interband hopping increases: if an electron from the c band hops to the f band, there is an energy increase due to the double occupancy of the f band and the Coulomb repulsion; conversely, if an electron from the f band hops to the c band, the energy increase is due to the site energy, ε_f. Thus, the overall effect is a decrease in the effective hybridization with increasing U, as shown by the square data points in Fig. 2(b). However, the hybridization correlation shows an inflection point at $U^{\times} \simeq 2.2$, as indicated by the sign change in its second derivative (circles). Figure 2(b) also shows the on-site magnetic correlation between the two bands (squares). For small U, the behavior is dominated by the increase of f-band magnetic moments, but before reaching $U^{\times}$, the magnetic interband correlations are already affected by the decrease in the effective hybridization.

Let us now examine magnetic correlations. Figure 2(c) shows the magnetic structure factor for the f-band electrons on a 40-site lattice. While the peak is always located at $q = \pi$, indicating the presence of antiferromagnetic correlations, its height increases with U, signaling the strengthening of the correlations. The peak heights are shown in Fig. 2(d) as functions of the inverse lattice size. For small U, they are very weakly dependent on N_s, indicating short-ranged correlations. For $U = 6$, on the other hand, the peaks grow with lattice size, indicating long-ranged correlations. In-between these two limits we observe a smooth crossover, in which the peak heights become more dependent on the lattice size as U is increased.

Figure 2(e) shows the log-linear plot of the real-space magnetic correlations of the f electrons. It shows that the decay of the correlations is exponential, confirming the lack of quasi-long-range order, but there is also a large increase in the correlation length ξ, with U. From a fit to the form $S_f(r) \sim e^{-r/\xi}$, we determine $\xi(U)$, which is shown in Fig. 2(f). We see that above $U \simeq 2$, ξ increases exponentially with U, indicating a rapid growth in the range of the magnetic correlations; one should also note that this crossover in the behavior of the correlation length occurs in the very same region as the crossovers discussed in connection with Figs. 2(a) and 2(b). The symmetric PAM also displays a spin gap at half filling (not shown; see, e.g., Ref. 8), so that this exponential decay of magnetic correlations should be interpreted as a manifestation of a spin-liquid phase, similar to the behavior of ladder systems with an even number of legs, for which an exponential decay of spin-spin correlations is produced by a finite spin gap.[23] The magnetic correlations for c electrons follow a similar pattern.

The picture that emerges is that the symmetric PAM at half filling is a spin liquid for all $U > 0$, but with a steady strengthening of antiferromagnetic correlations beyond $U^{\times}$. This picture is also consistent with previous results obtained through other numerical methods, such as exact

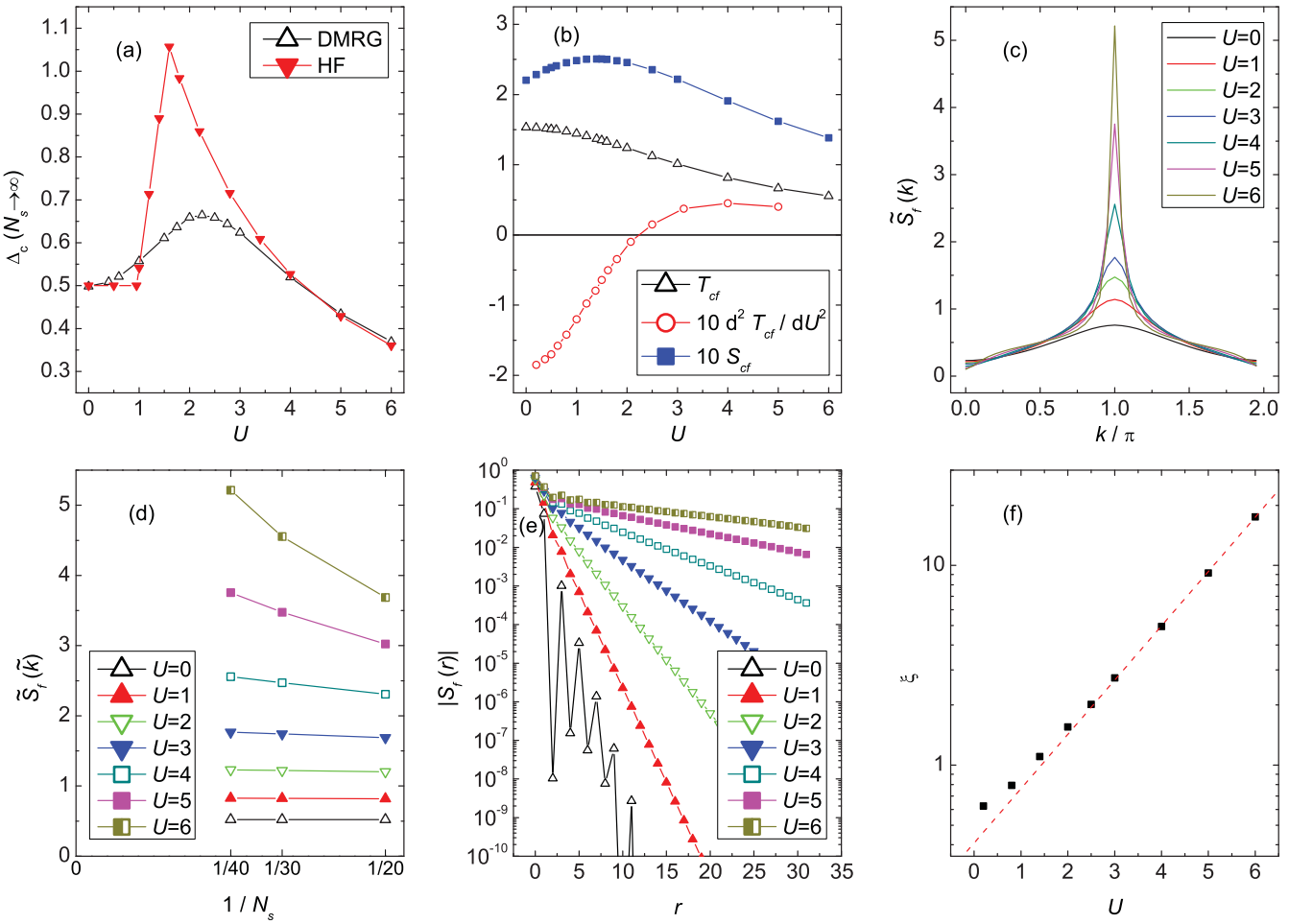

FIG. 2. (Color online) Half filling: $n = 2$. (a) Comparison of the charge gap obtained with Hartree Fock and from our DMRG results. The DMRG points are the outcome of a linear extrapolation ($N_s \to \infty$) from data for lattices with $N_s = 20$, 30, 40 and 50 sites. (b) Hybridization correlation, its second derivative, and the on-site magnetic correlation between c and f bands for $N_s = 40$. (c) f-band magnetic structure factor for $N_s = 40$. (d) Size dependence of the height of the f-band magnetic structure factor peaks. (e) Log-linear plot of the absolute value of the f-band real-space magnetic-correlation function for $N_s = 40$. (f) The U dependence of the correlation length extracted from (e), as explained in the text; the dotted line is the corresponding exponential fit.

diagonalization[22,24,25] and quantum Monte Carlo,[26] or mean-field theories.[4,27–29]

IV. QUARTER FILLING ($n = 1$)

In the noninteracting case at quarter filling, the Fermi energy lies within the lower branch of $E_-(k)$, as indicated in Fig. 1, so that the system is a paramagnetic metal; this leads to a vanishing charge gap when $U = 0$. A finite-size scaling analysis of our DMRG data indicates that there are three regimes for the gap. For $0 \leqslant U \lesssim 2$, it scales linearly with N_s^{-1}, so that it extrapolates to zero, as $N_s \to \infty$. For $2 \lesssim U \lesssim 4$, the gap approaches a finite value in the thermodynamic limit, but we cannot ascertain whether the behavior follows an inverse linear dependence (B/N_s, with decreasing slope B) or a nonlinear form, $N_s^{-\alpha}$, with α continuously varying between 1 and 1.5. And finally, for $U \gtrsim 4$ the gap is hardly dependent on the system size. In Fig. 3(a), the extrapolated values are shown, which are suggestive of a metal insulator transition (MIT) taking place at $U_{c1} \simeq 2$.

The MIT could have bearings on the hybridization and on-site magnetic correlations, Eqs. (5) and (6). Figure 3(b) shows that as U increases from 0, these interband correlations increase until they reach a maximum at U_{c1}. Beyond this point, they both decrease, but while the hybridization correlations are still present even for large U, on-site magnetic correlations become negligible for $U \gtrsim 8$. This decoupling is due to the decrease in occupation of the c band when U increases. At quarter filling there is only one electron per site, shared between both bands. As we increase U, the f band lowers in energy (through the increase of magnitude of ε_f) and the electron becomes more localized in the f band. This is illustrated in the same figure: as U increases, the average f-band occupation $\langle n_f \rangle$ also increases, and the average c-band occupation $\langle n_c \rangle$ decreases, with their sum being constant and equal to 1. In the limit of $U \gg V$, there is one electron on the f band at each site, and the c band will be empty, thus rendering S_{cf} negligible.

Let us now discuss the magnetic behavior of both c and f subsystems. Figure 3(c) shows the magnetic structure factor

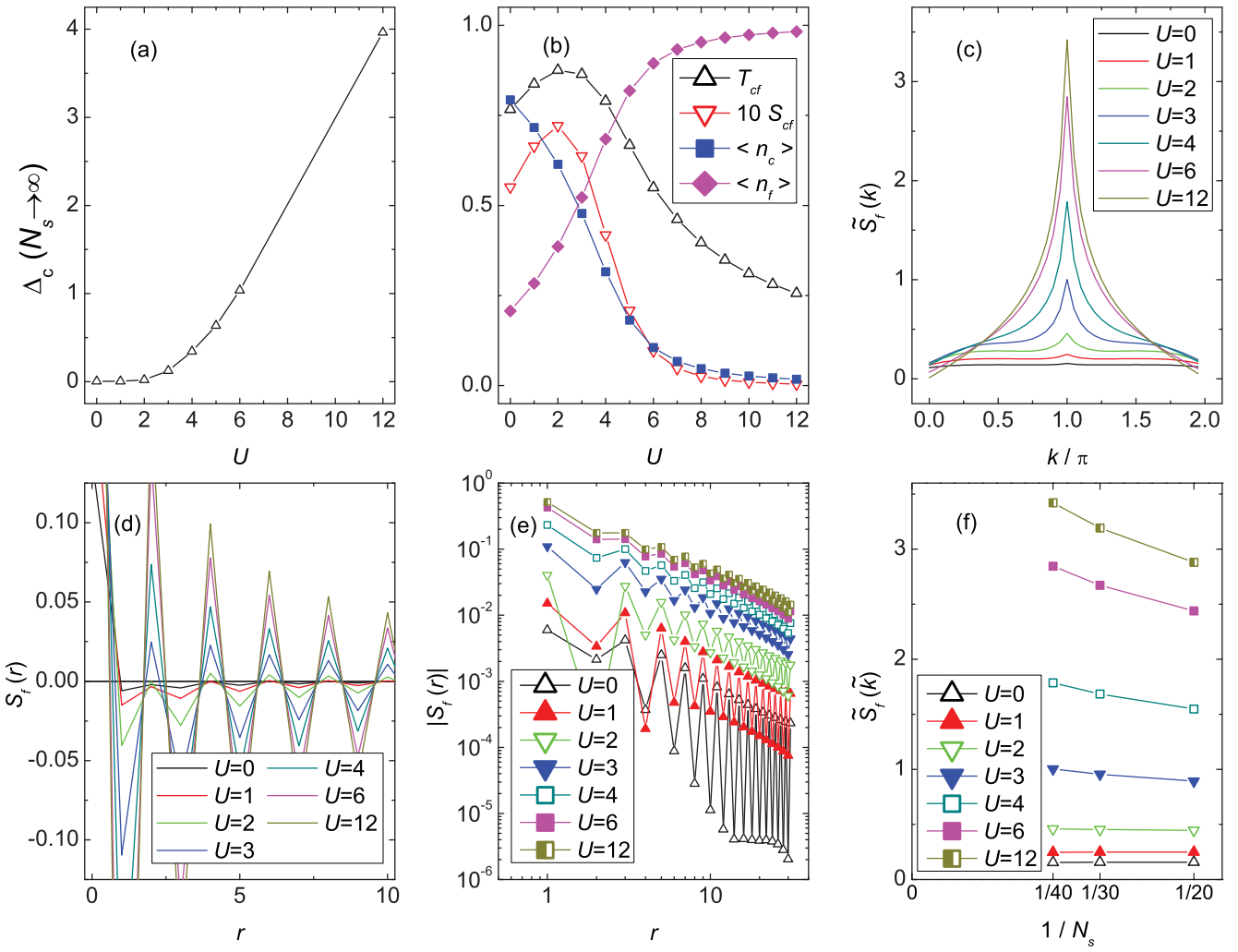

FIG. 3. (Color online) Quarter filling, $n = 1$. (a) The charge gap as a function of U: data are the outcome of extrapolations ($N_s \to \infty$) from data for lattices with $N_s = 20$, 30, 40, and 50 sites. (b) On-site correlations between c and f bands (hybridization and magnetic, Eqs. (5) and (6), respectively) and average charge density of each band for $N_s = 40$. (c) f-band magnetic structure factor for $N_s = 40$. (d) Real-space f-band magnetic correlations for $N_s = 40$. (e) Log-log plot of the absolute value of the f-band real-space magnetic correlations for $N_s = 40$. (f) Size dependence of the height of the f-band magnetic structure factor peaks.

for the f electrons, for several values of U. We see that the peak positions do not depend on U, being all located at $k = \pi$: the correlations are predominantly antiferromagnetic. By contrast, their intensity is strongly dependent on U. In order to understand this, we first examine these correlations in real space [Fig. 3(d)]: while for $U < 2$ the correlations are very short ranged, consistent with a paramagnetic state, above $U = 2$ their amplitude increases considerably and their range is significantly more extended. In Fig. 3(e) we plot the magnitude of the correlation function on a log-log scale, from which we see that very noisy (and of very small magnitude) data for $U < 2$ turn into steady straight lines for $U \gtrsim 2$, following a power law in $1/r^{\alpha}$, which is the signature of a spin-density wave. The power-law exponent α decreases steadily with U from $\alpha \simeq 1.1$, for $U \simeq 2$, to $\alpha = 1$, for $U \simeq 4$, remaining constant and equal to 1 for larger U.

One should also note that the peak of $\tilde{S}(k)$ scales with the system size. In Fig. 3(f) we plot the size dependence of the peak height for the f-band magnetic structure factor, for different values of U. The peaks do not grow with system size below $U_{c1} \simeq 2$, consistently with a paramagnetic state. Above U_{c1}, the peaks show an increase with the lattice size, which is to be associated with the longer range of the magnetic correlations.

Similar magnetic behavior is verified for the c-band magnetic correlations, i.e., antiferromagnetic correlations and power-law decay (not shown). However, contrary to what happens in the f band, the c-band magnetic correlations reach a maximum at $U \simeq 3$ and start to decrease. This decrease can be attributed to the behavior of the c-band occupation. As shown in Fig. 3(b), the occupation of the c band decreases as U increases, and in the limit of $U \gg V$ the c band is empty. In this case, the c-band magnetic correlations are zero, and the f-band magnetic correlations are generated by an effective superexchange interaction generated by virtual electrons hopping to the c band.

For quarter filling, one may envisage a transition at $U_{c1} \simeq 2$, from a paramagnetic metal to an insulator with an f-band spin-density wave; in this context, our data therefore refines a

previous mean-field approach,[29] while adding more accurate information to previous DMRG work.[15] Nonetheless, since the evolution with U of both the gap and the spin correlations is somewhat smooth at small U, one cannot entirely exclude the possibility of a quite small U_{c1}.

V. INTERMEDIATE FILLINGS

In this section we discuss what happens to the ground state of the PAM as we dope away from the special densities, quarter fillings, and half fillings. In order to draw a somewhat accurate phase diagram, we have obtained the ground state for fillings $n = 1.125$, 1.25, 1.375, 1.5, 1.75, and 1.875; for each filling, we are constrained to work with different system sizes, in such a way that the number of electrons could be exactly fitted in the lattice. For example, for $n = 1.125$ we did the calculations for systems with $N_s = 16$, 32, and 48 sites, and $N_e = 18$, 36, and 54 electrons, respectively, while for $n = 1.25$, they had $N_s = 24$, 32, 40, and 48 sites, and $N_e = 30$, 40, 50, and 60 electrons, respectively.

In the noninteracting case, the picture is similar to what happens for quarter filling: the Fermi energy lies on the lower branch of $E(k)$ (see Fig. 1), and the system is a paramagnetic metal. However, contrary to what happens for quarter filling, there is no charge gap even after U is switched on (not shown), so the system is always a metal. On the other hand, the magnetic properties of the ground state can be completely different, depending on the filling factor and on the values of U. In what follows, we focus primarily on the behavior for $n = 1.25$ and 1.75; for other fillings the picture is qualitatively similar to either of these, though the actual magnetic boundaries in the phase diagram do depend on the values of n.

We start by examining what happens for $n = 1.25$: in Fig. 4(a) we plot the f-band magnetic structure factor for different values of U. When $U = 0$, the structure factor is featureless, as expected for a paramagnet; this behavior persists up to $U_c \simeq 4$. For $U > U_c$, a sharp peak in the structure factor appears at $k = 0$, indicating the emergence of a ferromagnetic

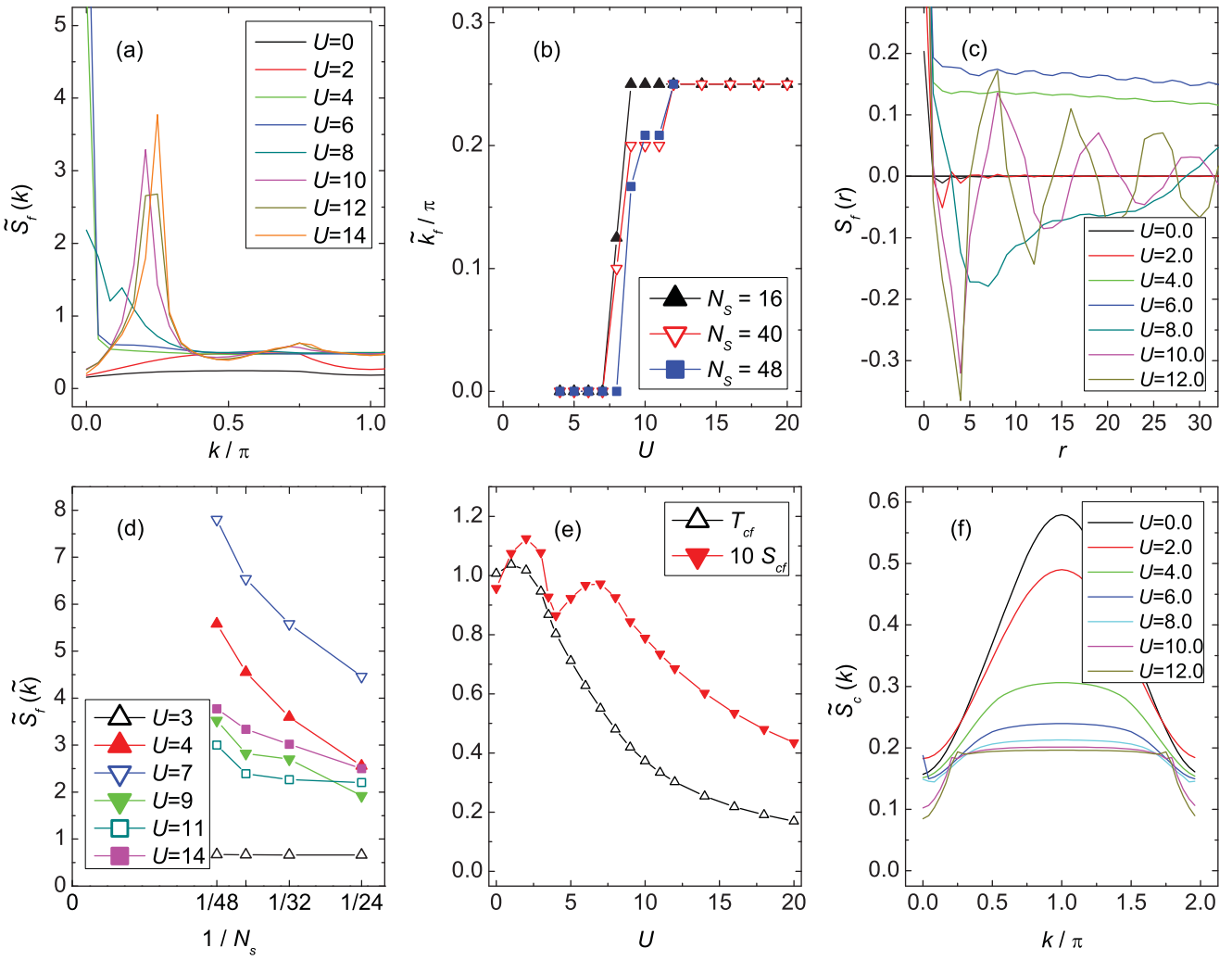

FIG. 4. (Color online) Intermediate filling, $n = 1.25$. (a) Structure factor for the f-band magnetic correlations for $N_s = 48$. (b) Peak position (normalized by π) of the f-band magnetic structure factor, as a function of U. (c) Real-space f-band magnetic correlations for $N_s = 48$. (d) Size dependence of the height of the f-band magnetic structure factor peaks. (e) Hybridization correlation and the on-site magnetic correlation between c and f bands for $N_s = 40$. (f) Structure factor of the c-band magnetic correlations for $N_s = 48$.

phase. This peak remains at $k = 0$ up to $U \simeq 8$, when it starts moving toward higher values of k (now with another peak located symmetrically relative to $k = \pi$). The evolution of the peak position, $\tilde{k}_f$, with U is shown in Fig. 4(b) for three different system sizes. We see that for very large values of U, $\tilde{k}_f$ stabilizes at $\pi/4$. The origin of this specific value can be traced back to the occupation of the conduction band. Indeed, for $n = 1.25$, with $V = 0$ and for U large enough, the f band accommodates one electron per site, while the c-band occupation is $n_c = 0.25$; the Fermi wave vector for the conduction band is therefore given by $2k_F^c = \pi n_c = \pi/4$. In the spirit of the RKKY interaction, when V is switched on, the oscillatory behavior of the effective interaction between the f moments is set exactly by the Fermi momentum of the conduction band; hence, $\tilde{k}_f = 2k_F^c$, and this has been referred to as the RKKY phase.[15]

Between the ferromagnetic and RKKY phases, $\tilde{k}_f$ grows with U, as can be seen from Fig. 4(b); the corresponding evolution with U of the magnetic correlations in real space is displayed in Fig. 4(c). The changing of $\tilde{k}_f$ with U is reflected in the continuous change in the period of oscillation of the correlations, as shown in Fig. 4(c). One should also note that the appearance of an intermediate plateau in the plot of $\tilde{k}_f(U)$ around $U \sim 10$ in the cases of $N_s = 40$ and 48, should be taken as suggestive that as the lattice size increases, the plateaus will narrow so that curves will grow monotonically, starting from $\tilde{k}_f = 0$ for $U \simeq 8$, and reaching $2k_F^c$ at $U \simeq 12$ [see Fig. 4(b)]. We therefore conclude that as U increases, the system goes from the FM phase to the RKKY phase through an intermediate incommensurate spin-density-wave (ISDW) phase.

The robustness of these three different magnetic arrangements can be checked through the analysis of the size dependence of their structure factor peaks, shown in Fig. 4(d). For $U = 3$, the peak remains constant as the lattice is increased, consistently with the absence of magnetic ordering or a paramagnetic state. For the other values of U—which correspond to the different magnetic arrangements FM, ISDW, and RKKY—we see that the peak increases with the size of the lattice, indicating long-range correlations.

It is interesting to connect these transitions with the hybridization and on-site magnetic correlations, Eqs. (5) and (6), and shown in Fig. 4(e). In the PM phase, the hybridization correlation first increases, and starts decreasing before the FM phase sets in; it then decreases steadily as U increases. On the other hand, the magnetic correlations carry on increasing, reaching a maximum at a higher value of U, although still smaller than $U_c \simeq 4$. Therefore, the onset of a FM state results from a delicate balance between hybridization and magnetic correlations. However, once the f moments form the FM state, their on-site correlation with the spins of the conduction electrons start increasing again; at the PM-FM transition, T_{cf} has an inflection point. At $U_I \simeq 7$, S_{cf} reaches a maximum, suggesting that the onset of the ISDW phase results from a weakening of the on-site magnetic correlations; however, no signature of the FM-ISDW is seen on T_{cf}. Interestingly, as U increases further, no signature of the ISDW-RKKY transition is seen in either T_{cf} or S_{cf}; perhaps other intersite correlation functions would show some signature.

We now discuss the magnetic correlations of the c electrons. The fact that the structure factor displays broad maxima [see Fig. 4(f)] instead of sharp peaks is due to the absence of direct effective interaction between the conduction electrons: spins on neighboring sites are antiferromagnetically correlated, but these correlations hardly extend beyond the nearest-neighbor distance; hence, there is no quasiordering. Nonetheless, for large U the f band is so strongly correlated that the c electrons start feeling its residual effects through their hybridization with the f band; that is, the range of magnetic correlations of c electrons increases considerably. A closer look at Fig. 4(f) reveals small peaks appearing at exactly the same positions of those in the f-band magnetic structure factor: $q = 0$ for $U = 6$ and 8, $q = 0.21\pi$ for $U = 10$, and $q = 0.25\pi$ for $U = 12$, thus indicating that the conduction electrons track the ordering of the f moments; however, due to their itinerant character and reduced mean occupation, the correlations are considerably weaker than those between f electrons.

From the above analysis, the picture for $n = 1.25$ is that the system is metallic, and as U is increased, it goes through four different magnetic phases. Initially, for U close to zero, the system is paramagnetic. As U is increased, it undergoes a transition to a ferromagnetic phase, which, as U is further increased, is replaced by a phase with strong incommensurate spin-density-wave magnetic correlations, and eventually the system enters a phase with RKKY correlations for sufficiently strong U.

One should note that this ISDW phase had been predicted through a slave-boson approach,[4] but was not found in early DMRG calculations:[15] due to the limited system sizes used (up to 16 sites) in that work, the resolution of the magnetic structure factor was $\Delta\tilde{k}_f = 0.125\pi$, which is not narrow enough to distinguish the ISDW peak from the one expected for RKKY correlations; this resolution was only attained with the large systems considered here.

The picture described above is similar for all densities examined up to $n = 1.5$; in every case we have identified the same four magnetic phases. However, for $n \geqslant 1.75$ the picture is quite distinct: the ferromagnetic phase is no longer present. Figure 5(a) shows the peak positions, $\tilde{k}_f$, of the structure factor as a function of U. There is a region between $U = 1$ and $U = 2$ in which the peak is located at $\tilde{k}_f = 0.25\pi$, but as shown in Fig. 5(b), for $U \leqslant 3$ the peaks are independent of the system size, indicating the absence of strong magnetic correlations. Above $U \simeq 3$, $\tilde{k}_f$ rises toward the value expected for RKKY interactions, $\tilde{k}_f = 0.75\pi$, but similarly to what happens for $n \leqslant 1.5$, the system goes through an ISDW phase. It is also instructive to compare the behavior of the on-site interband correlations, $S_{cf}(U)$ and $T_{cf}(U)$: the discontinuity in the first derivative of the former, which accompanied the onset of the FM phase in Fig. 4(e), is no longer present for $n = 1.75$. Therefore, apart from the suppression of the ferromagnetic phase, the remainder of the phase diagram is unchanged for densities greater than $n = 1.5$, and can still be divided into three regions, corresponding to PM, ISDW, and RKKY phases.

Before closing our discussion, a few remarks are in order. First, we call attention to the presence of small peaks at $k = 0.75\pi$ for a few values of U ($U = 2$, for example) in Fig. 4(a). These peaks might be due to the presence of an extended Fermi surface, to which both the c and f electrons contribute and should be taken into account when calculating the Fermi wave number. In this case, for $n = 1.25$, the peak in the magnetic

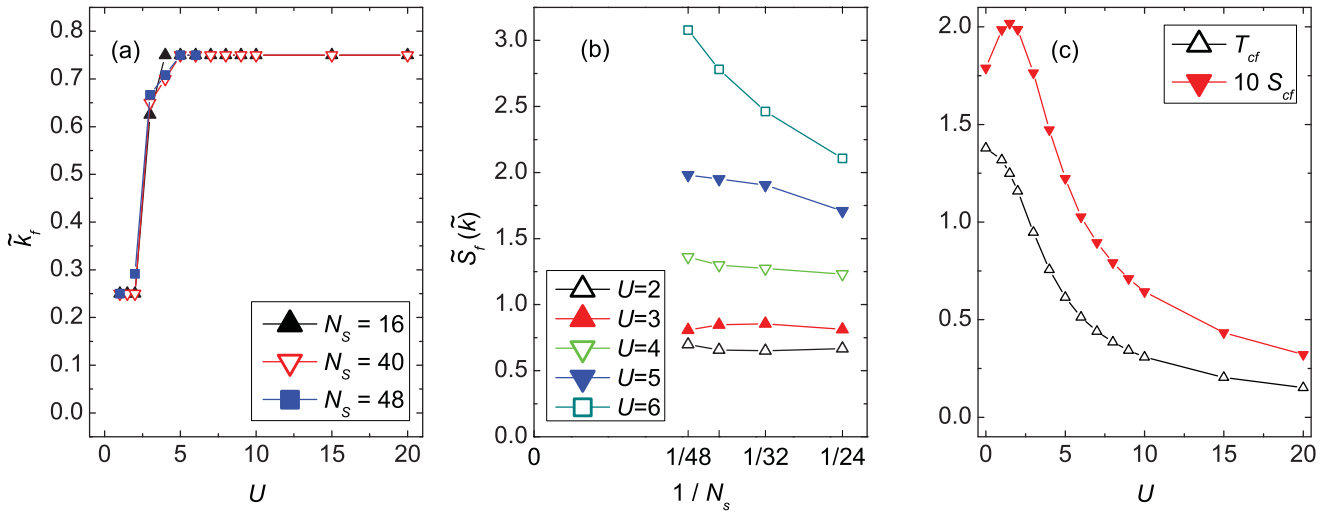

FIG. 5. (Color online) Intermediate filling, $n = 1.75$. (a) Peak position (normalized by π) of the magnetic structure factor for f-band electrons. (b) Size dependence of the height of the f-band magnetic structure factor peaks. (c) On-site hybridization and magnetic interband correlations for $N_s = 40$.

structure factor would be expected to be at $2k_F = \pi n = 1.25\pi$ and 0.75π (since the structure factor is symmetric around π), instead of $2k_F^c$. This would also explain the maxima of the structure factor at $k = 0.25\pi$ for $n = 1.75$ and $U < 3$ in Fig. 5(a). However, these peaks do not grow with the lattice size. Secondly, for $n = 1.125$, we have identified a small region within the ferromagnetic phase (close to the boundary for smaller values of U) in which the system phase separates into ferromagnetic and antiferromagnetic domains. These domains are quite apparent in the spatial-dependent magnetic correlation functions, where regions with ferromagnetic correlations are intercalated with regions with spin-density wave (SDW) correlations, as previously reported in Ref. 16; however, since this only happens in a very narrow region of the phase diagram, we have not attempted to determine the boundaries. A similar phase separation has also been reported for the Kondo lattice model with ferromagnetic Hund's coupling, in which near half filling, there is a region of the phase diagram in which the ferromagnetic phase gives place to a phase-separated regime with hole-undoped antiferromagnetic and hole-rich ferromagnetic regions.[30] Thirdly, the appearance of another ferromagnetic region close to $n = 1.75$ has been suggested in Ref. 31; this phase would be analogous to the one obtained for the Kondo lattice model in Ref. 32. In view of this, we have carried out thorough tests for $n = 1.75$ and 1.875 in order to detect such a phase, but all our results were negative.

VI. CONCLUSION

In conclusion, we have carried out extensive (i.e., for lattices up to 50 sites) DMRG studies of the one-dimensional periodic Anderson model for several electronic densities between $n = 1$ (quarter filling) and $n = 2$ (half filling). Our main results are summarized in the phase diagram of Fig. 6, which settles several issues. For quarter filling, $n = 1$, the picture that emerges is consistent with a metal-insulator transition from a paramagnetic metal to an insulator with an f-band spin-density wave, at $U_{c1} \simeq 2$; however, the smooth evolution of the gap and the spin correlations does not entirely exclude the possibility that U_{c1} could actually be quite small. At half filling, $n = 2$, we have established that the magnetic correlations decay exponentially with distance for all $U > 0$, so that the system is always an insulating spin liquid, but with a steady strengthening of correlations beyond $U^\times \simeq 2$; that is, in the Kondo regime, the correlation length grows exponentially with U.

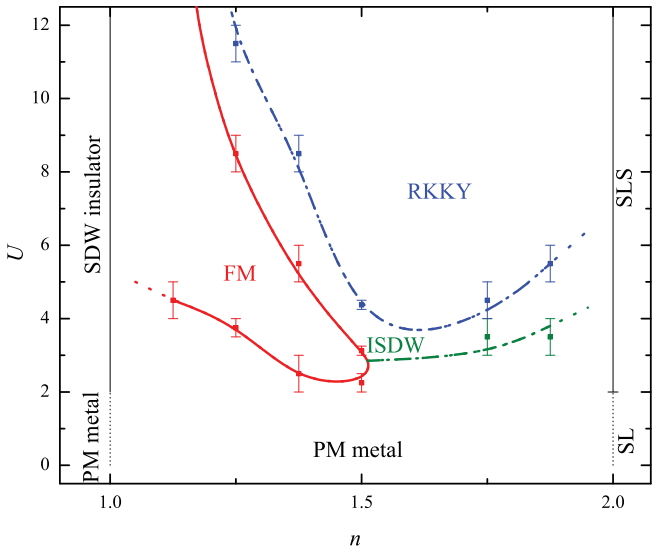

FIG. 6. (Color online) Phase diagram for the PAM at fixed hybridization, $V = 0.75$. The f electrons can be found in one of the following magnetic states: paramagnetic (PM), spin-density-wave (SDW), ferromagnetic (FM), incommensurate spin-density-wave (ISDW), and a SDW with momentum determined by the Fermi momentum of the conduction electrons (RKKY; see text); SL and SLS stand for spin liquid and spin liquid with strong antiferromagnetic fluctuations. The lines for $1 < n < 2$ are guides to the eye. Solid lines indicate actual phase transitions, whereas dash-dotted lines denote changes in the dominating correlations.

For $1 < n < 2$, the system is always metallic, but the magnetic behavior is quite diverse. For $U \lesssim 3$ the system is paramagnetic, indicating that charge fluctuations dominate the processes, even in the metallic state. As U increases above this threshold, the f levels lie sufficiently deep into the conduction band to stabilize local moments. As one dopes away from quarter filling, keeping U fixed, the excess electrons go into the conduction band, but form local singlets with those in the f states;[4,5] it is then energetically favorable for the local singlets to move in a ferromagnetic background if the conduction band is not too full. As the doping increases, the singlet gas becomes denser and the above picture breaks down, destroying the ferromagnetic background; by the same token, for fixed electronic density, the singlets become less stable as U increases, and the FM phase is destroyed.

On the other hand, if one removes electrons from half filling for U sufficiently strong, the conduction electrons mediate the interaction between the localized f spins, leading to a SDW with a magnetic wave-vector spin determined by the occupation of the conduction band; this is the RKKY regime. As U decreases below a certain value, charge fluctuations disturb this role played by the conduction electrons, and while the system still sustains a SDW, its wave vector is incommensurate (ISDW) with the underlying lattice. Interestingly, this ISDW phase is also present in the low-density side, but it now appears as an intermediate phase between the FM and the RKKY.

As a final remark, we should recall that superconductivity in heavy fermions appears when pressure is applied; effects of pressure could, in principle, be mimicked by varying the PAM parameters. However, no indications of superconducting correlations in the PAM have been found so far in a wide range of parameters. In view of this, one possible route to discuss the coexistence between magnetic order and superconductivity in heavy fermions is to introduce additional couplings to the PAM, which would stabilize pairing; coexistence of superconductivity with local moments has been successfully addressed in Ref. 33 within this approach.

ACKNOWLEDGMENTS

Financial support from the Brazilian Agencies FAPERJ, FAPESP, and CNPq (through fellowships and grants) is gratefully acknowledged.

[1] P. W. Anderson, Phys. Rev. **124**, 41 (1961).
[2] A. C. Hewson, *The Kondo Problem to Heavy-Fermions* (Cambridge University Press, Cambridge, England, 1997).
[3] C. Bastide and C. Lacroix, J. Phys. C **21**, 3557 (1988).
[4] B. Möller and P. Wölfle, Phys. Rev. B **48**, 10320 (1993).
[5] T. Yanagisawa, Phys. Rev. Lett. **70**, 2024 (1993).
[6] K. Ueda, H. Tsunetsugu, and M. Sigrist, Phys. Rev. Lett. **68**, 1030 (1992).
[7] G.-S. Tian, Phys. Rev. B **50**, 6246 (1994).
[8] M. Guerrero and C. C. Yu, Phys. Rev. B **51**, 10301 (1995).
[9] C. M. Varma, Phys. Rev. B **50**, 9952 (1994).
[10] S. R. White, Phys. Rev. Lett. **69**, 2863 (1992).
[11] S. R. White, Phys. Rev. B **48**, 10345 (1993).
[12] U. Schollwöck, Rev. Mod. Phys. **77**, 259 (2005).
[13] K. A. Hallberg, Adv. Phys. **55**, 477 (2006).
[14] A. L. Malvezzi, Braz. J. Phys. **33**, 55 (2003).
[15] M. Guerrero and R. M. Noack, Phys. Rev. B **53**, 3707 (1996).
[16] M. Guerrero and R. M. Noack, Phys. Rev. B **63**, 144423 (2001).
[17] M. A. Ruderman and C. Kittel, Phys. Rev. **96**, 99 (1954).
[18] T. Kasuya, Prog. Theor. Phys. **16**, 45 (1956).
[19] K. Yosida, Phys. Rev. **106**, 893 (1957).
[20] E. H. Lieb and F. Y. Wu, Phys. Rev. Lett. **20**, 1445 (1968).
[21] D. J. Garcia, K. Hallberg, B. Alascio, and M. Avignon, Phys. Rev. Lett. **93**, 177204 (2004).
[22] T. Nishino and K. Ueda, Phys. Rev. B **47**, 12451 (1993).
[23] E. Dagotto and T. Rice, Science **271**, 618 (1996).
[24] R. Jullien and R. M. Martin, Phys. Rev. B **26**, 6173 (1982).
[25] K. Ueda, J. Phys. Soc. Jpn. **58**, 3465 (1989).
[26] R. Blankenbecler, J. R. Fulco, W. Gill, and D. J. Scalapino, Phys. Rev. Lett. **58**, 411 (1987).
[27] M. M. Steiner, R. C. Albers, D. J. Scalapino, and L. J. Sham, Phys. Rev. B **43**, 1637 (1991).
[28] C. Papatriantafillou, N. Kioussis, and S. H. Park, Phys. Rev. B **60**, 13355 (1999).
[29] Y. Luo and N. Kioussis, Phys. Rev. B **65**, 195115 (2002).
[30] S. Yunoki, J. Hu, A. L. Malvezzi, A. Moreo, N. Furukawa, and E. Dagotto, Phys. Rev. Lett. **80**, 845 (1998).
[31] I. P. McCulloch, Ph.D. thesis, Australian National University, (2001).
[32] I. P. McCulloch, A. Juozapavicius, A. Rosengren, and M. Gulacsi, Phys. Rev. B **65**, 052410 (2002).
[33] P. R. Bertussi, A. L. Malvezzi, T. Paiva, and R. R. dos Santos, Phys. Rev. B **79**, 220513 (2009).